Epitaxial growth of ordered and disordered granular sphere packings

Andreea Panaitescu and Arshad Kudrolli*
Department of Physics, Clark University, Worcester, Massachusetts 01610, USA
(Received 25 March 2014; published 3 September 2014)

We demonstrate that epitaxy can be used to obtain a wide range of ordered to disordered granular packings by simply changing the deposition flux. We show that a defect-free face-centered-cubic (fcc) monocrystal can be obtained by depositing athermal granular spheres randomly into a container with a templated surface in a gravitational field without direct manipulation. This packing corresponds to the maximum sphere packing fraction and is obtained when the substrate is templated corresponding to the (100) plane of a fcc crystal and the container side is an integer multiple of the sphere diameter. We find that the maximum sphere packing is obtained when the deposited grains come to rest, one at a time, without damaging the substrate. A transition to a disordered packing is observed when the flux is increased. Using micro x-ray computed tomography, we find that defects nucleate at the boundaries of the container in which the packing is grown as grains cooperatively come to rest above their local potential minimum. This leads to a transition from ordered to disordered loose packings that grow in the form of an inverted cone, with the apex located at the defect nucleation site. We capture the observed decrease in order using a minimal model in which a defect leads to growth of further defects in the neighboring sites in the layer above with a probability that increases with the deposition flux.

DOI: 10.1103/PhysRevE.90.032203 PACS number(s): 45.70.Qj, 81.05.Rm

Granular materials when poured into a container in a gravitational field quickly dissipate away their kinetic energy and come to rest because of inelastic collisions and friction between grains. Even in the case of monodisperse spherical particles, the resulting packings are disordered [1,2] with a packing fraction that has been shown with numerical simulations [3] to depend on the grain-grain friction. Reducing the kinetic energy of the particles being deposited is thought to result in looser packings [4,5]. If the container is vibrated or tapped, such packings only approach a random close packing fraction of approximately 0.64 [2], well below the maximum sphere packing fraction $\phi_{\max}$ of $\sqrt{2}\pi/6 \approxeq 0.74$ corresponding to an ordered structure.

Meanwhile, templating and epitaxy has been used to grow ordered atomic thin films [6,7] and colloidal crystals with a single phase [8,9]. The development of order and defects can vary in principle depending on the flux and temperature, which determine the degree of thermalization in the surface layer as the particles come to rest [10]. In the case of granular matter that is athermal, it has been shown that packings with random hexagonal-close-packed (rhcp) or fcc symmetry can be observed if the container is vibrated horizontally while spheres are slowly poured [11,12]. However, a large number of defects could also be observed, making it unclear if it is possible to make fully ordered granular packings without direct manipulation.

Here, we demonstrate that a defect-free monocrystal can be obtained by simply adding monodisperse particles at random onto a templated substrate, provided the deposition rate and energy are sufficiently small, and in fact vibrations are unnecessary. The key idea is that the deposited spheres come to rest one at a time, which allows them to fall to the potential minimum before being obstructed by other spheres. We obtain internal scans of the packing with micro x-ray computed tomography, and we show how cooperative locking of spheres above their local minima leads to defects at the container boundary when the deposition energy is increased. We characterize the orientational order using statistical measures corresponding to each sphere, and we show that fcc is the only ordered phase.

In our experiments, the template corresponds to gravitational potential wells created in a square grid with spheres in contact corresponding to the (100) plane of a fcc crystal. We choose this template because it can give rise in principle to a monocrystal (whereas a hexagonal template gives rise to a rhcp structure due to the degeneracy of the A and C planes of a hcp structure with respect to its B plane). With the spheres thus arranged in a square lattice, a sphere placed on this layer will have the highest gravitational potential energy at points precisely above the center of the spheres in the layer below, and minimum potential energy directly above where the diagonals joining lattice points in the layer below meet. The potential energy difference ΔU for a unit mass gives a relevant energy scale for the kinetic energy of the spheres being deposited, and is given by $\Delta U = (1 - \sqrt{2/3})gd$, where g is the gravitational acceleration and d is the sphere diameter. Granular spheres, when deposited, bounce a few times before completely losing kinetic energy, unlike atoms and colloids which are thermally activated. Spheres that are being deposited with sufficiently large energies can also dislodge and damage the substrate. *A priori* it is difficult to predict if such defects heal when additional spheres are added or lead to further defects.

Our experiments are performed using 5698 plastic spheres with diameter $d = 5.90 \pm 0.04$ mm in a laser-cut acrylic container with a $15d \times 15d$ square inner cross section. The plastic beads have a coefficient of restitution $e = 0.82 \pm 0.2$ and sliding friction $\mu_s = 0.33 \pm 0.03$. A square lattice of holes with diameter $d_h = 1.8$ mm with a spacing d is drilled into the bottom surface of the container such that spheres placed in the holes correspond to the (100) plane of a fcc packing. Once the template is constructed, we deposit the spheres by hand from a height h above the top layer with a random position in the

*Author to whom all correspondence should be addressed: akudrolli@clarku.edu

 ©2014 American Physical Society

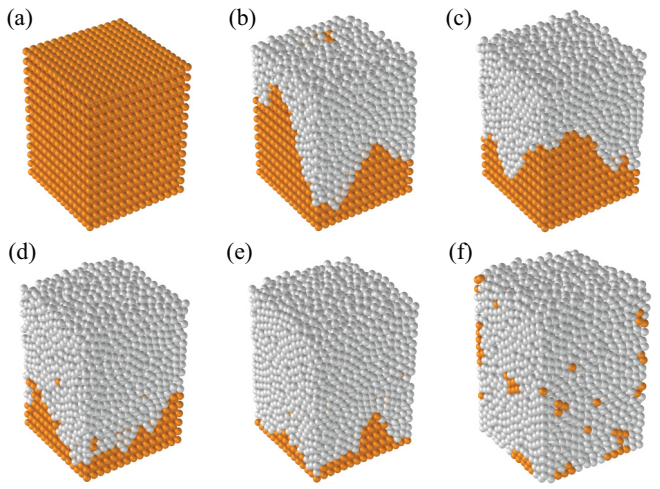

FIG. 1. (Color online) (a) A fully ordered fcc packing observed by dropping spheres for sufficiently low deposition flux $\Gamma = 11$, which is normalized by the template potential well energy. A transition to disordered packings is observed as the deposition flux is increased to $\Gamma = 16$ (b), $\Gamma = 22$ (c), $\Gamma = 109$ (d), and $\Gamma = 1090$ (e). (f) Example of a disordered packing observed when all the spheres are dropped from a height of the container where $\Gamma = 3.6 \times 10^5$. The spheres are rendered using their measured positions with ordered [orange (light gray)] and disordered (gray) phase denoted by using $Q_{6,\mathrm{local}}$ as a criterion.

horizontal plane. Thus a scaled deposition flux is given by the total deposition energy E scaled by the depth of the potential well ΔU, i.e., $\Gamma = E/\Delta U = \frac{nh}{(1-\sqrt{2/3})d}$, where n is the number of spheres dropped simultaneously. In the experiments we discuss in the following, $n = 1$, 2, 10, 100, and 5698.

After each packing is prepared, it is scanned with a Varian Medical Systems microfocus x-ray computed tomography instrument. The position of the spheres is measured to within the sphericity of the particle diameters using the centroid of the voxels corresponding to each sphere. The total packing fraction ϕ is then calculated by using the average of the highest layer of spheres in the container. Further, we also use Voro++ [13] to obtain the Voronoi cells corresponding to the volume closest to each particle in the packing. This allows us to identify nearest neighbors that share a face of their Voronoi cells as well as those that neighbor the boundaries of the container. By considering Voronoi cells that do not share a face with a boundary, we also obtain the volume fraction in the bulk of the packing ϕ_{bulk}.

A sample set of packings obtained as a function of increasing deposition flux is shown in Figs. 1(a)–1(f). Here the packings are rendered using the measured sphere positions and are further marked according to whether they are considered ordered or disordered, using the local orientational order parameter $Q_{6,\mathrm{local}}$ as a criterion (see Appendix). To investigate the internal structure of the packings, we plot the number density of the spheres ρ averaged over $0.3d$ thick horizontal transects as a function of distance z from the substrate in Figs. 2(a)– 2(f). This averaging distance was chosen to be smaller than the plane-plane distance in a fcc/hcp so that the contribution due to each plane can be resolved. The packings obtained by dropping spheres one at a time from a height $h \sim 2d$ and random horizontal positions are shown in Fig. 1(a). In this case, the granular spheres being deposited collide with those that form the substrate, then roll and slide down the potential well before coming to rest at the bottom. Even though $\Gamma \approx 11$, the deposited spheres do not appear to move or damage the substrate layer. The density plot in Fig. 2(a) corresponding to the ordered packing shows clear periodic oscillations with narrow peaks that alternate with two different amplitudes. These amplitudes are consistent with the growth of a fcc packing with 225 and 196 spheres in alternate horizontal planes corresponding to the dimensions of the container.

It may also be noted that the total volume fraction ϕ is measured to be 0.68 by using the height of the top layer of beads and the lateral dimensions of the container, which is lower than ϕ_{max}. However, this difference arises because of the side walls of the container, which prevent placement of spheres in partially filled sites. Thus, when we calculate the volume fraction ϕ_{bulk} using Voronoi cells that do not share a face with the packing boundary, we find $\phi_{\mathrm{bulk}} = 0.73$, which is within experimental error of ϕ_{max}.

As the normalized deposition flux Γ is increased, the packing can be observed to transition from an ordered to a disordered phase. This is demonstrated by considering the packing obtained by dropping spheres sequentially from $h = 3d$ in Fig. 1(b) with $\phi_{\mathrm{bulk}} = 0.67$, by dropping two spheres at a time from a height of $h \sim 2d$ in Fig. 1(c) with $\phi_{\mathrm{bulk}} = 0.65$, and by dropping 10 and 100 spheres at a time from a height of $h \sim 2d$ in Figs. 1(d) and 1(e) with $\phi_{\mathrm{bulk}} = 0.64$. Further, a packing obtained by pouring all the spheres rapidly from the top of the container is shown in Fig. 1(f). This last case is similar to how granular packings are typically prepared, and the resulting $\phi_{\mathrm{bulk}} = 0.60$ is similar to those previously reported with glass spheres [14].

From Figs. 1(b)– 1(d), we observe that the packing is initially ordered and becomes disordered with height as indicated also quantitatively by the decrease in amplitude of oscillation of $\rho(z)$ in Figs. 2(b)– 2(d). The decay of layering occurs increasing rapidly as Γ is increased, and in the case of the highest Γ it decays exponentially away from the boundary, similar to previous studies of packing near boundaries using the particle-interstitial liquid refractive index matching technique [15]. One can further note that while the amplitude of ρ oscillations decreases, the height of the packing grows higher. This is consistent with the fact that disordered packings have lower packing fractions compared with ϕ_{max}.

To examine the nature of the packing at the level of an individual sphere, we plot $Q_{4,\mathrm{local}}$ versus $Q_{6,\mathrm{local}}$ for each individual sphere in Fig. 3 for the six different packings. In Fig. 3(a), the points are closely clustered around the values corresponding to a finite-sized fcc crystal (see Appendix). The probability distribution function (PDF) of the $Q_{6,\mathrm{local}}$ plotted in the inset shows a narrow peak corresponding to the bulk value for a fcc crystal, whereas in Fig. 3(f), the points appear scattered over a broad range of values. Examining the corresponding inset, one notes that the sharp peak corresponding to the bulk value of $Q_{6,\mathrm{local}}$ is absent and, instead, a broader distribution that can be fitted by a Gaussian is observed. Such a distribution has been shown to be consistent with a packing with uncorrelated angular

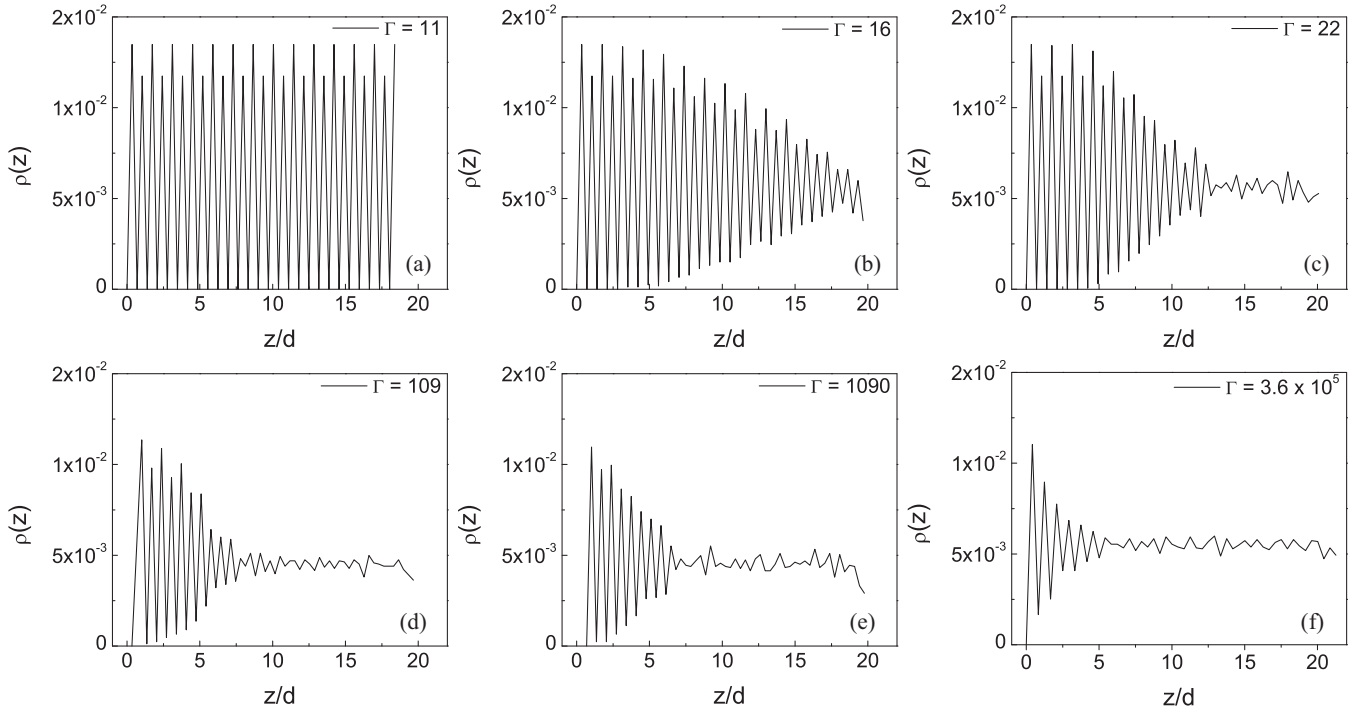

FIG. 2. (a)–(f) The density profile $\rho(z)$ as a function of height z corresponding to packings shown in Figs. 1(a)– 1(f).

distribution of neighbors [16]. The plots of $Q_{4,\mathrm{local}}$ versus $Q_{6,\mathrm{local}}$ [see Figs. 3(b)– 3(e)] corresponding to packings with an order-to-disorder transition show a scatter of points similar to the random case as well as values clustered around the

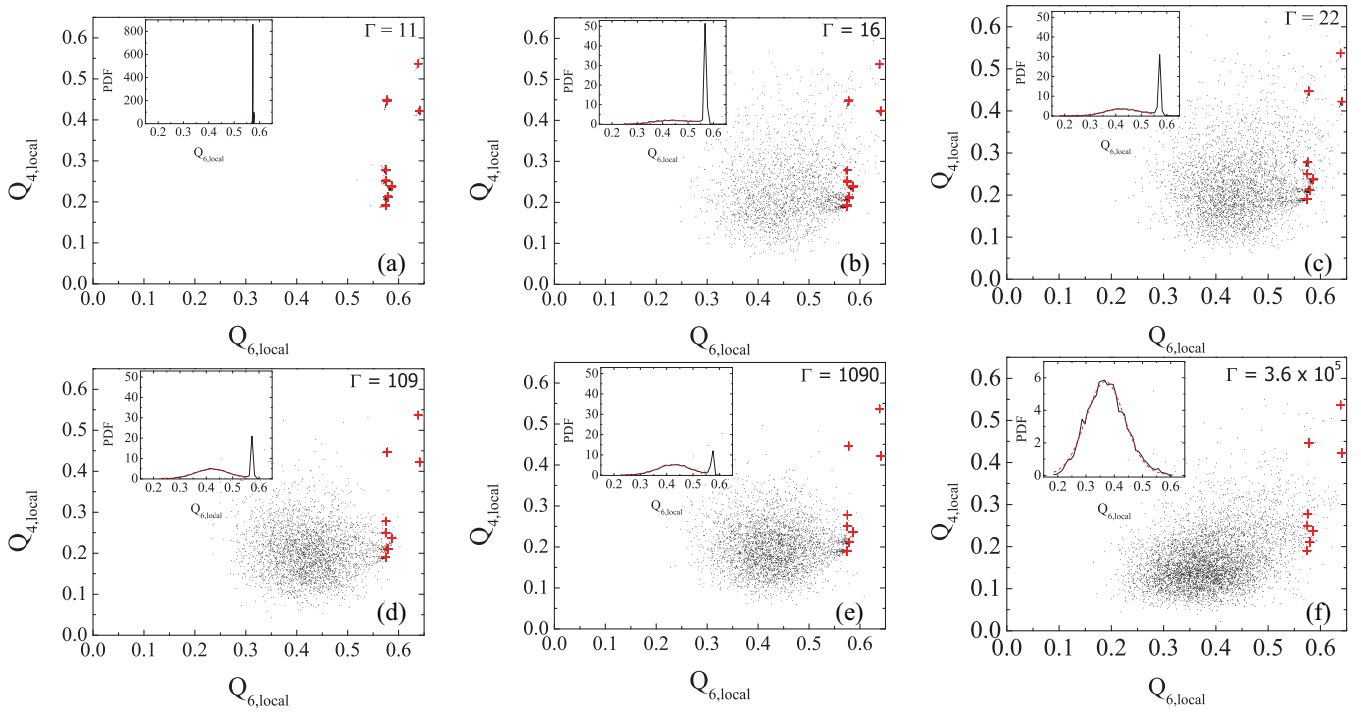

FIG. 3. (Color online) (a)–(f) The scatter plot of $Q_{4,\mathrm{local}}$ vs $Q_{6,\mathrm{local}}$ corresponding to packings shown in Figs. 1(a)– 1(f). Each point corresponds to a particular sphere in the packings. The expected values for a fcc monocrystal of the size of the container is indicated by a red +. Insets: the corresponding probability distribution function (PDF) of $Q_{6,\mathrm{local}}$. (a) A sharp peak is observed corresponding to the theoretical $Q_{6,\mathrm{local}}$ in the bulk of a fcc monocrystal, and a much smaller peak due the ones next to the boundaries. As the deposition flux Γ is increased, the fcc peak is observed to decrease in value, and a broader distribution is observed that is fitted by a Gaussian [dashed red (gray) line] with mean 0.45 (b), 0.43 (c), 0.42 (d), and 0.43 (e). (f) The fcc peak is observed to be completely absent and the distribution is fitted by a Gaussian with mean 0.37.

fcc crystal. Examining the PDFs, one can note that the sharp fcc peaks decrease in amplitude and broaden. Further, a second peak that can be well fitted to Gaussian distribution is observed. The means obtained by fitting these distributions are slightly shifted compared to the distributions observed in the case of the packing, which are fully disordered. We assume that this occurs because of the presence of partial ordering when calculating $Q_{6,\mathrm{local}}$ for spheres on the boundary between ordered and disordered regions. Furthermore, it can be noted that no other peaks corresponding to other symmetries (such as hexagonal close packing) are observed. This is in contrast with partially ordered packings obtained by applying shear, in which a mixture of fcc and hcp phases is observed at comparable volume fraction [14]. Thus, the packings obtained by epitaxial growth contain only domains of spheres with fcc order, random order, and partial order corresponding to the interface between the fcc ordered and disordered regions.

In the case of spheres, defects can arise in multiple ways. In addition to the locus of maxima and minima which are arranged in a square lattice [which are denoted by crosses and circles, respectively, in Fig. 4(a)], the center of the line joining lattice points correspond to saddle points. Because granular particles have friction, a small area $\approx\mu^2 d^2$ around the maxima and saddle points is in fact stable, where μ is the coefficient of rolling friction between the spheres. If a sphere has sufficient initial energy to overcome the friction, then it will move to a neighboring local minimum before coming to rest. Because $\mu \approx 10^{-4}$ in the case of the plastic spheres used in our experiments, this area of stability is in fact small and thus the probability for the formation of such individual defects appears to be small. However, as the energy of the spheres being deposited is increased with Γ, they can cause the spheres in the substrate to move and even dislodge completely. In this case, it becomes more probable that the spheres collectively come to rest slightly above their local minimum because of frictional frustration at contacts. If a sphere in the substrate is not precisely touching the side wall of the cell, then the saddle point corresponding to that sphere and its neighbor and the side wall becomes a shallow minimum (see Fig. 4). Thus, a sphere can get lodged in that minimum giving rise to a defect. This minimum can in turn give rise to further defects in its neighborhood, as it can prevent spheres from falling into its lattice location, as indicated in Fig. 4(b). Such defects are difficult to heal and lead to the growth of disorder in the layer above.

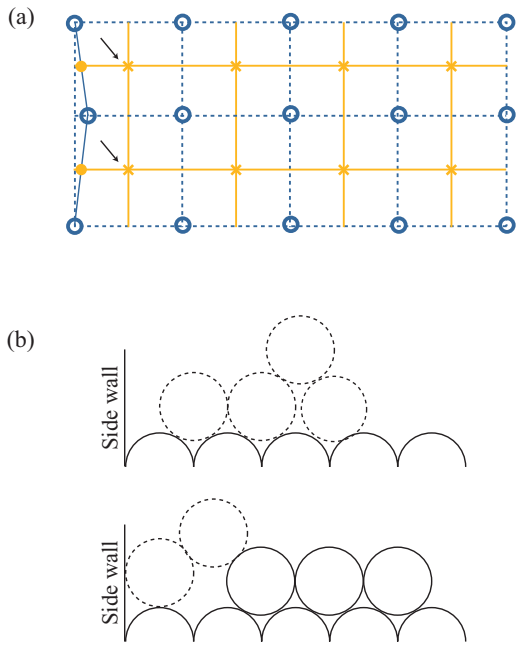

FIG. 4. (Color online) (a) Top view of the (100) plane of a fcc crystal with open blue (dark gray) circles and orange (light gray) cross symbols denoting the lattice sites in consecutive planes. The sites linked by dashed blue (dark gray) lines correspond to layer A and solid orange (light gray) lines to layer B, respectively. A defect leading to one of the spheres being slightly off its potential minima and away from the side wall is shown as well. In this case, the two points indicated by the solid orange (light gray) circles form small minima in which spheres can lodge, leading to defects, which in turn can exclude spheres from lodging into sites indicated by arrows. (b) Examples of defects that can arise because of imperfections in the template are indicated by circles with dashed-line style. A wide range of incipient arches can be supported with granular spheres because of the presence of friction.

Figure 5 shows the number of ordered spheres as a function of height for various Γ. The corresponding layer-by-layer identification of the ordered and disordered spheres is presented as movies in the Supplemental Material [17]. For example, in the case of $\Gamma = 16$, it can be seen that a defect in the fcc lattice appears in the fourth layer, and the number of particles in a disordered state starts to increase with layer number. It is apparent that the defects nucleate more or less all at the boundaries, and these defects lead to growth of further disorder with layer number.

To understand the observed form of the number of ordered spheres as a function of height, we consider a minimal

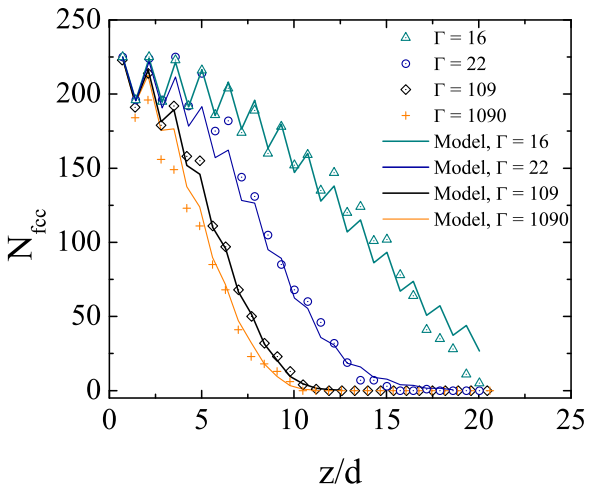

FIG. 5. (Color online) The number of ordered spheres as a function of height z is observed to decrease, increasing faster as the deposition flux is increased. The small layer-to-layer oscillation in each curve arises because the total number of fcc ordered spheres is different because of the finite size of the container. The overall trends are captured by a minimal model in which defects are nucleated at the boundaries, or by the presence of a defect in the layer below with a probability that increases with Γ (see text).

model of decay of order in a fcc lattice according to the following assumptions. Defects are assumed to nucleate only at the boundaries with a small probability, which depends on Γ. The presence of a defect is then assumed to lead to a defect in the nearest-neighbor site in the layer above with a significant probability that also depends on Γ. We implement the consequence of such a model by defining a three-dimensional (3D) matrix consisting of 28 alternating (15×15) and (14×14) matrices corresponding to each layer of the fcc lattice in which the elements are initialized to 1. Then, the elements at the boundary starting with the second layer are set at random to 0 with a probability corresponding to a probability P_n to find a nucleation site in the experiments. (The first layer is the template and thus has no defects.) Next, the matrix elements are considered layer by layer from the bottom up. If a matrix element corresponding to a defect is found, then it is assumed to lead to a defect in the nearest-neighboring site in the layer above with a probability P_p also measured from the experimental data corresponding to that particular Γ. In this case, that element is set to 0 as well. It may be noted readily from Fig. 4(b) that these nearest-neighboring sites are at a distance d and equal four in the bulk, and they can be as few as two at the boundaries. Iterating the consequence of this rule layer by layer, we now have a matrix with lattice points set to 1 corresponding to an ordered sphere, and those corresponding to defects as 0. We then obtain the decay of ordered sites by summing the elements layer by layer as a function of height. We simulate 100 such packings with defect sites selected randomly and then obtain an average decay of order for each Γ.

The results of the minimal model are shown in Fig. 5, where $P_n = 0.005$, 0.022, 0.034, and 0.049 and $P_p = 0.65$, 0.80, 1.0, and 1.0 for $\Gamma = 16$, 22, 109, and 1090, respectively. Because, we have only one experimental packing per Γ, it is difficult to interpret the values P_n and P_p except to note that P_n are small and P_p are large and increase with Γ. Nonetheless, one can clearly observe that the overall rapid decay of order is captured by the minimal model. This gives a simple mechanism by which order decays in the packing, and it shows that the disordered domains grow as inverted cones with the apex located near the side boundaries where the defects first nucleate. This picture is further confirmed from the profile view of packing in Figs. 1(b) and 1(c), where one can also observe that these disordered domains merge at large enough height to form a single disordered domain. The fact that defects nucleate at the boundaries in these examples implies that ordered layers can be easily obtained by using templates that are wider for even higher flux rates.

In conclusion, we have demonstrated that a fully ordered single crystal can be obtained by using the (100) plane of a fcc crystal as a template and by depositing monodisperse granular spheres with sufficiently low deposition rate and energy. Disorder is observed to nucleate at the boundaries due to cooperative locking of spheres in out-of-equilibrium positions. Thus, our experiments show that a fully ordered

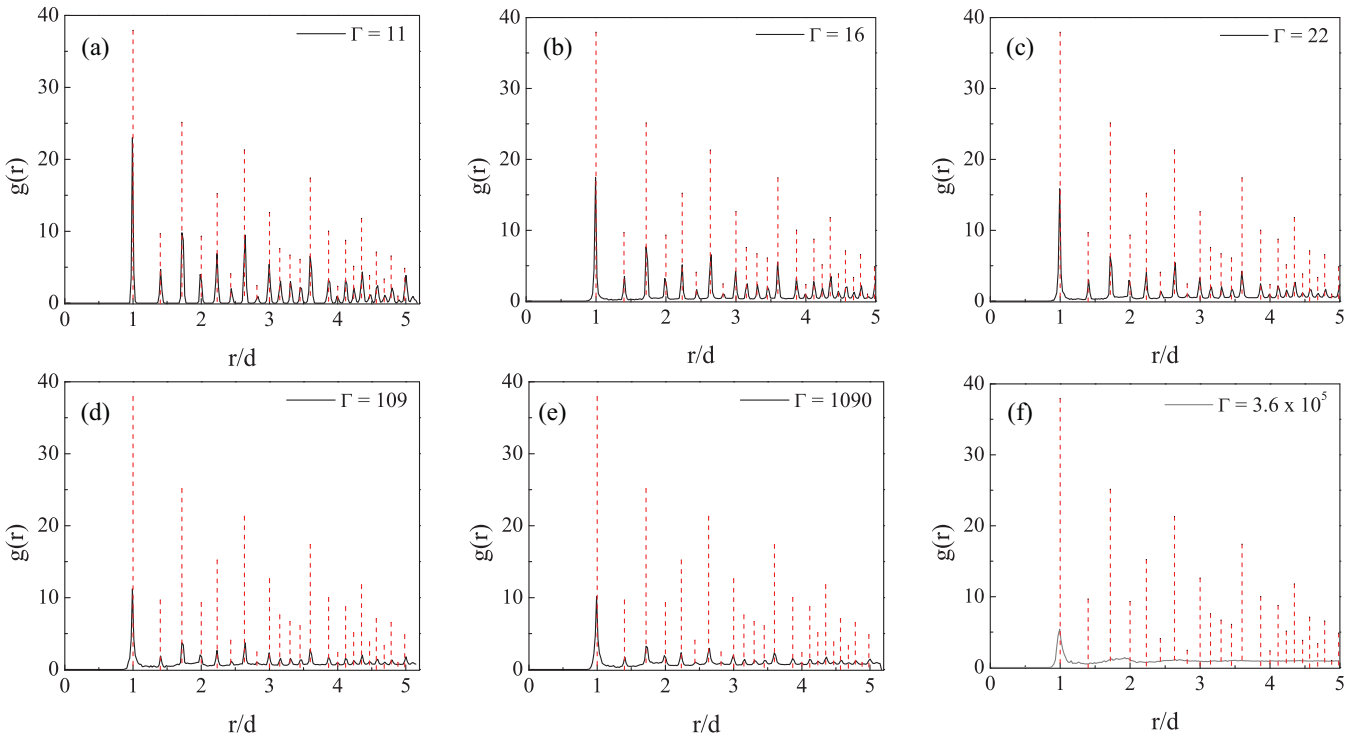

FIG. 6. (Color online) (a)–(f) The density-density radial correlation function for the six packings shown in Fig. 1, which span the fully ordered to random packings. The experimental data are compared and contrasted with the $g(r)$ obtained for a fcc packed crystal that fits in the container used in the experiments [the red (gray) dotted line]. The location of the peaks and the relative amplitude is observed to compare well in the case of the ordered packing. The peaks in the experiments are systematically lower and broader to the polydispersity and error in locating the center of the grains.

or disordered packing can be obtained by simply varying the deposition flux and the template.

We thank Mehran Kardar for stimulating discussions, and Vikrant Yadav and David Scheff for help with experiments. This work was supported by the National Science Foundation under NSF Grants No. CBET-0853943, No. DMR-0959066, and No. CBET-1335928.

APPENDIX: LOCAL ORIENTATIONAL ORDER PARAMETER

We use the orientation order metric to investigate orientational order in the packing. It is defined as

$$Q_{l,\mathrm{local}} \equiv \sum_{i=1}^{N} \left(\frac{4\pi}{l(l+1)} \sum_{m=-l}^{m=l} |\langle Y_{lm}(\Theta(\mathbf{r}), \Phi(\mathbf{r}))\rangle|^2 \right)^{1/2} \quad \text{(A1)}$$

where $l = 4,6$, Y_{lm} are the spherical harmonics, $\Theta(\mathbf{r})$ and $\Phi(\mathbf{r})$ are the polar and azimuthal angle, respectively, and $\mathbf{r}$ is the position vector from a particle to its neighbor [18]. We define particle neighbors using the density-density radial correlation function $g(r)$ as a function of distance r, and which is plotted in Fig. 6 for the six sample packings discussed. We consider all particles that fall below the first minimum observed beyond the peak. This definition removes the errors introduced when considering only neighbors in contact due to errors in finding the center of the spheres in the experiments.

To compare the packings observed in the experiments with an ideal fcc crystal with the same dimensions as the experimental container, we generate the positions corresponding to such a packing. We then compute the coordination number Z (the number of nearest neighbors), the local packing volume fraction, ϕ_{local}, and the local bond orientational parameter, $Q_{6,\mathrm{local}}$. These results are shown in Fig. 7. For an ideal infinite fcc lattice, in which each particle has 12 nearest neighbors, $Q_6^{\mathrm{fcc}} = 0.5745$ and the packing density is $\phi^{\mathrm{fcc}} = 0.74$ as in Fig. 7(a). The spheres situated on the surface layers of the crystal have fewer than 12 nearest neighbors, and consequently deviation from the expected value of Q_6^{fcc} and ϕ^{fcc} can be observed in those cases. Therefore, $Q_{6,\mathrm{local}}$ and ϕ_{local} for the particles at the boundary with fewer neighbors compared to those in the bulk are noted in Figs. 7(b)– 7(h).

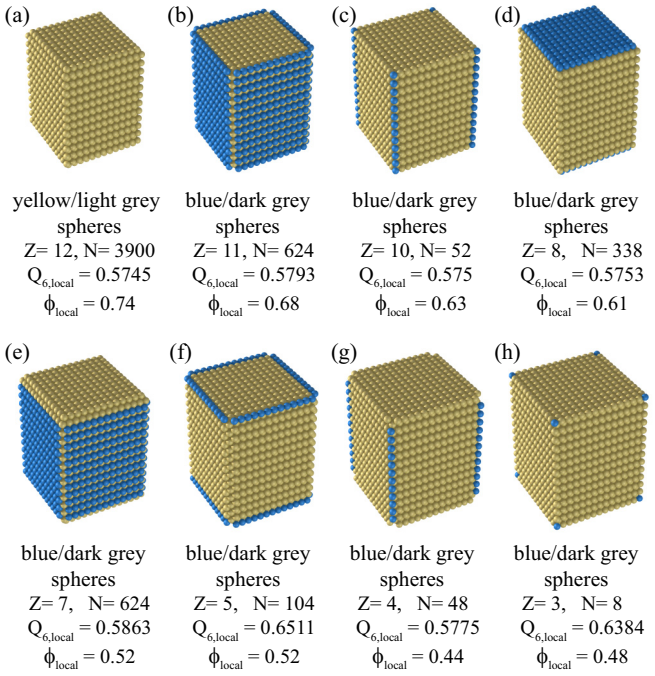

FIG. 7. (Color online) A computer-generated face-centered-cubic monocrystal: The particles are divided into eight categories based on their coordination number, Z, and the local packing volume fraction, ϕ_{local}, and bond orientational parameter, $Q_{6,\mathrm{local}}$, are reported for each category. N is the number of particles with the same Z. (a) The bulk particles have $Z = 12$ and $\phi_{\mathrm{local}} = \phi^{\mathrm{fcc}}$, $Q_{6,\mathrm{local}} = Q_6^{\mathrm{fcc}}$. (b)–(h) The spheres on the crystal surface have fewer than 12 nearest neighbors, and consequently deviation from the expected value of Q_6^{fcc} and ϕ^{fcc} can be observed in their case.

It can be noted that the local volume fraction decreases systematically when the coordination number decreases. However, the local bond order parameter $Q_{6,\mathrm{local}}$ does not change monotonically with coordination number. This is because the values of $Q_{6,\mathrm{local}}$ are determined not only by the relative positions of the neighbors but also by the number of nearest neighbors. Including the spheres at the boundaries also has a significant effect on the total volume fraction ϕ of the packing of this sample size. If one adds the ϕ_{local} contributions due to particles with $Z = 11$ and 10, as in Figs. 7(b) and 7(c), to those with $Z = 12$, the total packing fraction ϕ decreases to 0.73. Adding the contributions of all the particles in the packing yields $\phi = 0.68$.

[1] J. D. Bernal, Nature (London) **185**, 68 (1960).
[2] G. D. Scott and D. M. Kilgour, Brit. J. Appl. Phys. **2**, 863 (1969).
[3] L. E. Silbert, Soft Matter **6**, 2918 (2010).
[4] G. Y. Onoda and E. G. Liniger, Phys. Rev. Lett. **64**, 2727 (1990).
[5] G. R. Farrell, M. Martini, and N. Menon, Soft Matter **6**, 2925 (2010).
[6] B. Roas, L. Schultz, and G. Endres, Appl. Phys. Lett. **53**, 1557 (1988).
[7] S. Froyen and A. Zunger, Phys. Rev. Lett. **66**, 2132 (1991).
[8] A. Van Blaaderen, R. Ruel, and P. Wiltzius, Nature (London) **385**, 321 (1997).
[9] K. E. Jensen, D. Pennachio, D. Recht, D. A. Weitz, and F. Spaepen, Soft Matter **9**, 320 (2013).
[10] M. Kardar, Physica A **263**, 345 (1999).
[11] O. Pouliquen, M. Nicolas, and P. D. Weidman, Phys. Rev. Lett. **79**, 3640 (1997).
[12] A. B. Yu, X. Z. An, R. P. Zou, R. Y. Yang, and K. Kendall, Phys. Rev. Lett. **97**, 265501 (2006).
[13] C. H. Rycroft, Chaos **19**, 041111 (2009).

[14] A. Panaitescu, A. Reddy, and A. Kudrolli, Phys. Rev. Lett. **108**, 108001 (2012).

[15] A. V. Orpe, V. Kumaran, K. A. Reddy, and A. Kudrolli, Europhys. Lett. **84**, 64003 (2008).

[16] A. Panaitescu and A. Kudrolli, Phys. Rev. E **81**, 060301(R) (2010).

[17] See Supplemental Material at http://link.aps.org/Supplemental/10.1103/PhysRevE.90.032203 for movies showing the layer-by-layer formation of the packings which show order-to-disorder transition.

[18] P. J. Steinhardt, D. R. Nelson, and M. Ronchetti, Phys. Rev. B **28**, 784 (1983).